Electronic Supplementary Material (ESI) for Journal of Materials Chemistry A.
This journal is © The Royal Society of Chemistry 2021

Supporting information

Multifunctional bayberry-like composites consisting of CoFe encapsualted by carbon nanotubes for overall water splitting and zinc-air battery

Peifang Guo,[a] Renbing Wu,[*a] Ben Fei,[a] Jing Liu,[a] Da Liu,[a] Xiaoxiao Yan,[a] and Hongge Pan[*b,c]

[a] Department of Materials Science, Fudan University, Shanghai 200433, China

[b] State Key Laboratory of Silicon Materials and School of Materials Science and Engineering, Zhejiang University, Hangzhou 310027, P. R. China.

[c] Institute of Science and Technology for New Energy, Xi'an Technological University, Xi'an 710021, P. R. China

Experimental Section

Chemical and reagents: The potassium nitroferrocyanide ($Na_2Fe(CN)_5NO{\cdot}2H_2O$, 99%) reagent was obtained from Aladdin Co. Ltd.. The cobalt nitrate ($Co(NO_3)_2{\cdot}6H_2O$, 99%) reagent, ferric nitrate ($Fe(NO_3)_3{\cdot}9H_2O$, AR) reagent, and zinc nitrate ($Zn(NO_3)_2{\cdot}6H_2O$, AR) were obtained from Sinopharm Chemical Reagent Co. Ltd.. The commercial Pt/C (10%) catalyst was purchased from Aladdin Co. Ltd. and IrO_2/C (20%) catalyst was purchased from Adamas Reagent Co. Ltd. The KOH (AR) was obtained from Sinopharm Chemical Reagent Co. Ltd. Nafion (10%) was obtained from Aldrich Co. Ltd., and all the chemical reagents were used as received without further purification.

Preparation of A-Fe-PB-800 catalyst: The A-Fe-PB-800 catalyst was prepared by direct annealing of PB. The PB precursor was heated to 800 ℃ in nitrogen atmosphere and kept for 2 h, and then cooled down to room temperature naturally. The sample was then collected and denoted as A-Fe-PB-800.

Preparation of A-Co-ZIF-800 catalyst: The A-Co-ZIF-800 catalyst was prepared by mixing $Co(NO_3)_2{\cdot}6H_2O$ solution with dimethylimidazole solution and aging in dark for 2h, followed by annealing process. The sample was then collected and denoted as A-Co-ZIF-800.

Electrochemical measurements: All the electrochemical measurements were conducted on a CHI 760E electrochemical workstation (CH Instruments, Inc., Shanghai). The HER and OER performance were evaluated in 1.0 M KOH solution which was saturated with high-purity nitrogen using a three-electrode setup. The linear sweep

voltammetry (LSV) polarization curves for HER and OER were examined at the scan rate of 5 $mV \cdot s^{-1}$ in room temperature. The electrochemical impedance spectroscopy was carried out in the frequency range of 0.01 Hz ~100 kHz at –1.04 V (for HER) and 0.65 V (for OER), respectively. The cyclic voltammetry (CV) curves of the samples were collected in 1.0 M KOH solution from 0.47 V to 0.67 V *vs.* RHE for HER and from 1.07 to 1.27 V *vs.* RHE for OER at different scan rates (20, 40, 60, 80, and 100 mV s^{-1}). The long-term chronoamperometric measurements of HER and OER were performed at the corresponding potentials to deliver a current density of 10 mA cm^{-2}. All the measured polarization curve potentials were performed with iR compensation and were converted to reverse hydrogen electrode (RHE) by the calibration equation ($E_{vs.RHE} = E_{vs.SCE} + 0.2415\ V + 0.05916\ pH - iR_s$). The overall water splitting measurement was performed using a two-electrode system, in which two glassy carbon electrodes loaded with CoFe@N-CNTs-800 catalyst were used as both cathode and anode. For comparison, Pt/C and IrO_2/C were acted as cathode and anode catalysts, respectively.

The ORR measurements were conducted in O_2-saturated 0.1 M KOH solution using rotating ring-disk electrodes (RRDE). Before the LSV tests, 10 cycles of CV tests were performed to activate the catalysts, and the LSV curves were measured from 0.2 to 0.8 V with the disk rotation rate of 1600 rpm. For the Tafel plot, the kinetic current density measured at a rate of 10 mV s^{-1} with a rotating speed of 1600 rpm was calculated from the mass-transport correction of the RDE data by: $j_K = \frac{j_L \times j}{j_L - j}$, where j presents the measured current density, j_K and j_L are the kinetic- and diffusion-limiting current

densities. The $\%H_2O_2$ and the electron transfer number (n) were determined by the followed two equations: $\%H_2O_2=200\ i_r/(i_r/N+|i_d|)$ and $n=4Ni_d/(i_r+Ni_d)$, where i_d is disk current, i_r is ring current, and N is current collection efficiency of the Pt ring.

Density Functional Theory (DFT) Calculations: according to the previous reports, OER involves multiple proton-transfer processes as the following steps:

$$* + OH^- \rightarrow *OH + e^- \quad \text{(S-1)}$$

$$*OH + OH^- \rightarrow *O + H_2O + e^- \quad \text{(S-2)}$$

$$*O + OH^- \rightarrow *OOH + e^- \quad \text{(S-3)}$$

$$*OOH + OH^- \rightarrow *O_2 + e^- \quad \text{(S-4)}$$

$$*O_2 \rightarrow * + O_2 \quad \text{(S-5)}$$

in which the asterisk represents the surface of catalysts. During these steps, the various intermediates, e.g., *-OH, *-O, *-OOH, and *-O_2, are generated. The energetically favorable (100) surface of CoFe alloy was selected as the active regions. Furthermore, the free energy landscape of the intermediates during OER were calculated in different charge doping states. The free energy differences for each step (ΔG_i) during OER are theoretically calculated as following equations described:

$$\Delta \mathbf{G_1} = G(*OH) - G(*) - \mu OH = E(*OH) - E(*) - E(H_2O) + 1/2E(H_2) - eU + \Delta G_{H+}(pH) + \Delta(ZPE - T\Delta S) \quad \text{(S-6)}$$

$$\Delta \mathbf{G_2} = G(*O) - G(*OH) + \mu OH = E(*O) - E(*OH) - E(H_2O) + 1/2E(H_2) - eU + \Delta G_{H+}(pH) + \Delta(ZPE - T\Delta S) \quad \text{(S-7)}$$

$$\Delta \mathbf{G_3} = G(*OOH) - G(*O) - \mu OH = E(*OOH) - E(*O) - E(H_2O) + 1/2E(H_2) - eU + \Delta G_{H+}(pH) + \Delta(ZPE - T\Delta S) \quad \text{(S-8)}$$

$$\Delta G_{4,5} = 4*(1.23\ eV - eU + \Delta G_{H+}(pH)) - (\Delta G_1 + \Delta G_2 + \Delta G_3) \quad (S\text{-}9)$$

where U represents the potential obtained against the reversible hydrogen electrode (RHE) under standard conditions. According to the ΔG_H+(pH) = – k·BT log(pH), the change of Gibbs free energy for a proton relative to the pH is obtained. ΔG_i are calculated from zero-point energy (ZPE), entropy correction, and the DFT energy to $\Delta G_i = \Delta ZPE_i + \Delta E_i - \Delta T\Delta S_i$. To avoid the calculation including O_2(gas), which is difficult to calculated within the GGA-DFT scheme, the sum of $\Delta G_{1\text{-}5}$ was fixed at the experimental ΔG value (4.92 eV) in $2H_2O > 2H_2 + O_2$. Based on above analysis, the theoretical η could be calculated from the ΔG_i as the following equation presented:

$$\eta = \max(\Delta G_1, \Delta G_2, \Delta G_3, \Delta G_{4,5})/e - 1.23\ V \quad (S\text{-}10)$$

Similarly, as for the HER, the intermediate is *H. The Gibbs free energy change can be expressed as

$$\Delta G = E(*H) - E(*) - 1/2E(H_2) + \Delta(ZPE - T\Delta S) \quad (S\text{-}11)$$

Zinc-air battery Assembling: The air electrode was fabricated by casting the CoFe@N-CNTs-800 catalyst ink onto a hydrophobic carbon paper with the loading of 4.4 mg cm^{-2} and dried at room temperature for 24 h, while a polished Zn plate was applied as the anode. The 6.0 M KOH with 0.2 M $Zn(OAc)_2$ solution was used as the electrolyte. The open-circuit voltage and power density were measured on a CHI 760E electrochemical workstation. The galvanostatic discharge and charge cycle (10 min discharge and 10 min charge with a current density of 10 mA cm^{-2}), the specific capacity, and the energy density of the zinc-air battery were carried out on LANHE CT2001A.The specific capacity was calculated according to the equation: (capacity) / (weight of consumed

zinc). The energy density was calculated according to the equation: (energy) / (weight of consumed zinc).

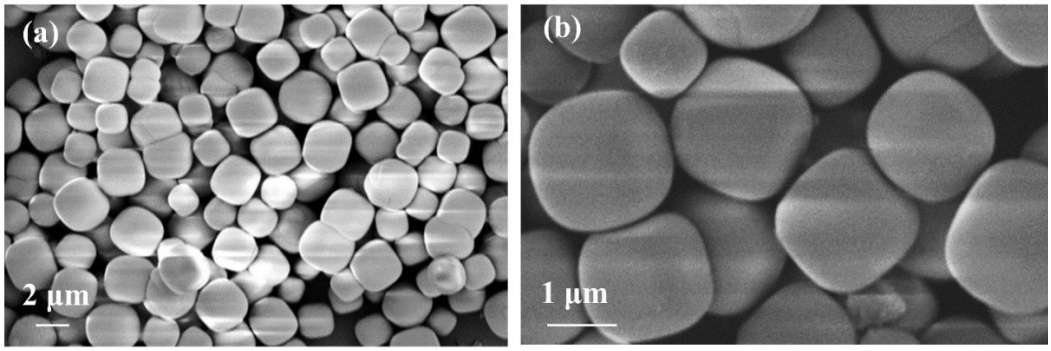

Fig. S1. FESEM images of CoFe-PBA.

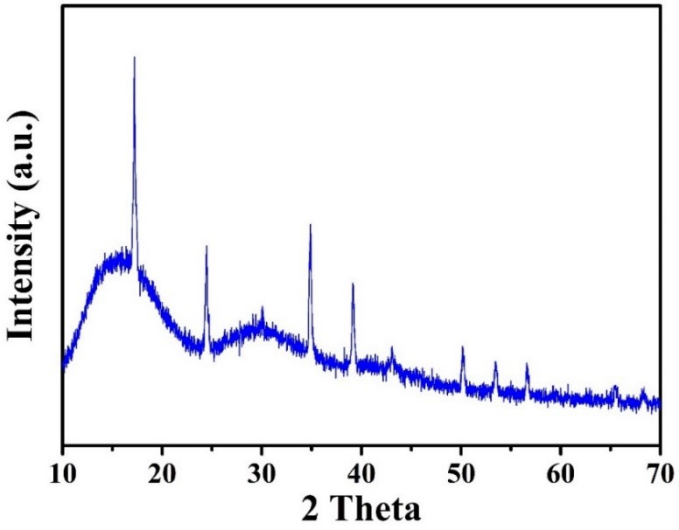

Fig. S2. XRD pattern of CoFe-PBA.

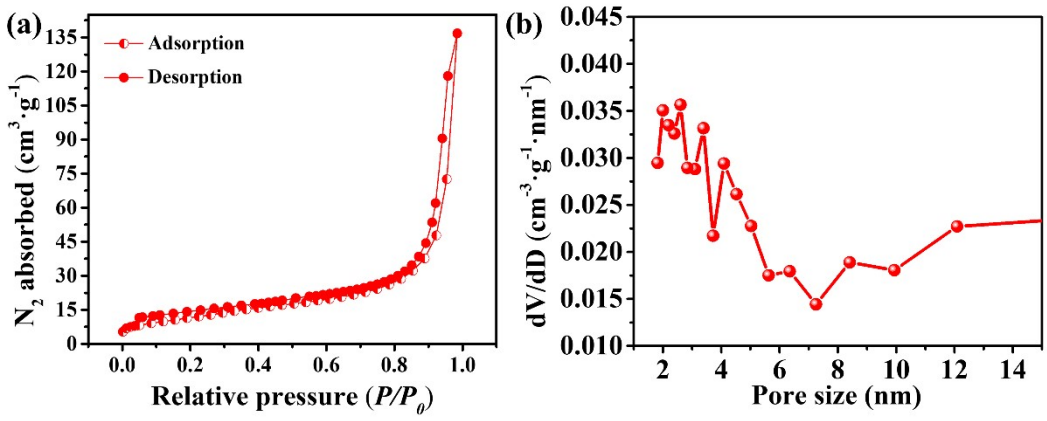

Fig. S3. (a) N_2 adsorption/ desorption isotherms curves of CoFe@N-CNTs-800 sample. (b) Pore width distribution calculated using the BJH method.

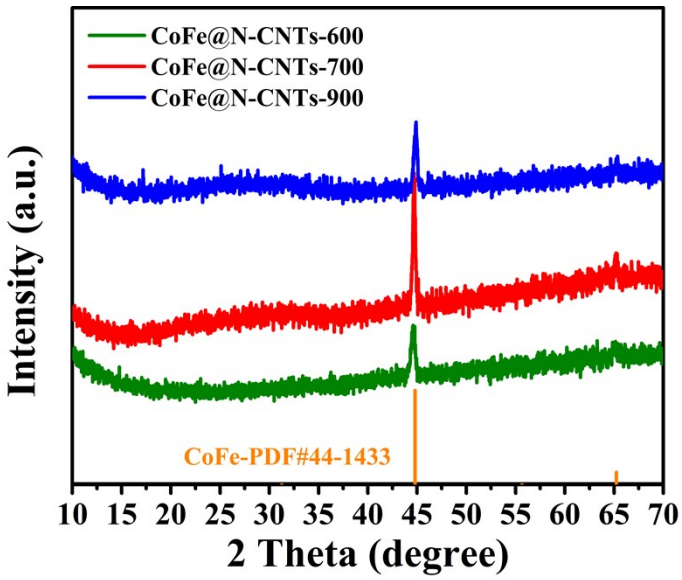

Fig. S4. XRD patterns of the as-prepared CoFe@N-CNTs samples obtained at different temperatures.

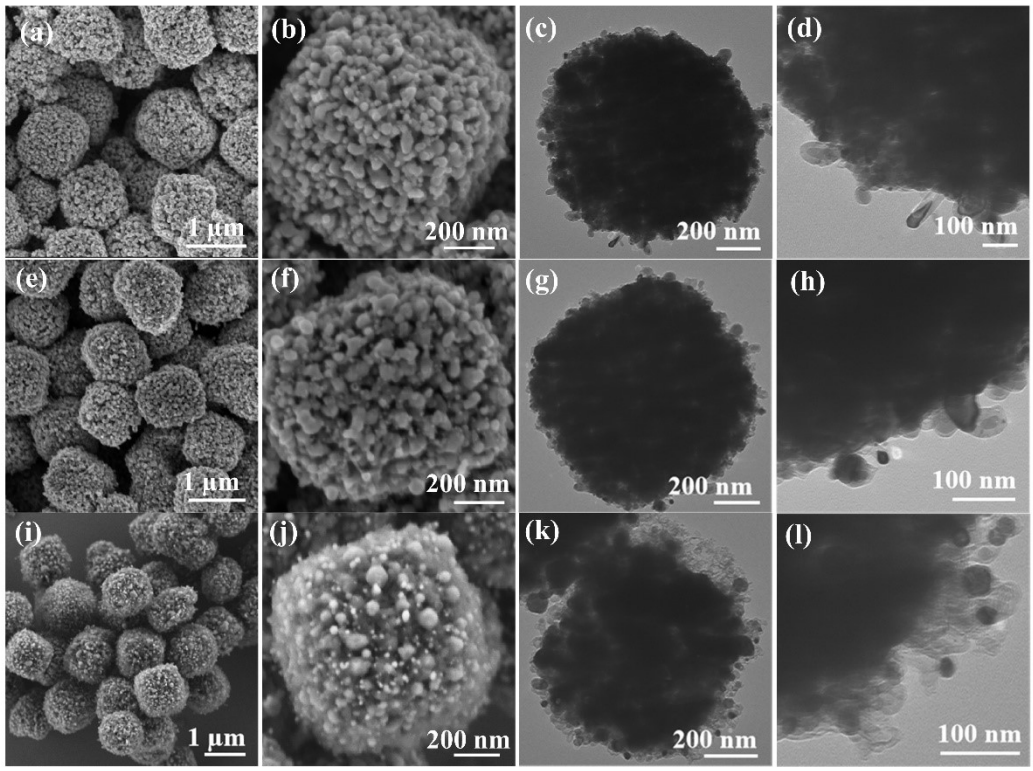

Fig. S5. FESEM and TEM images: (a)-(d) CoFe@N-CNTs-600. (e)-(h) CoFe@N-CNTs-700. (i)-(l) CoFe@N-CNTs-900.

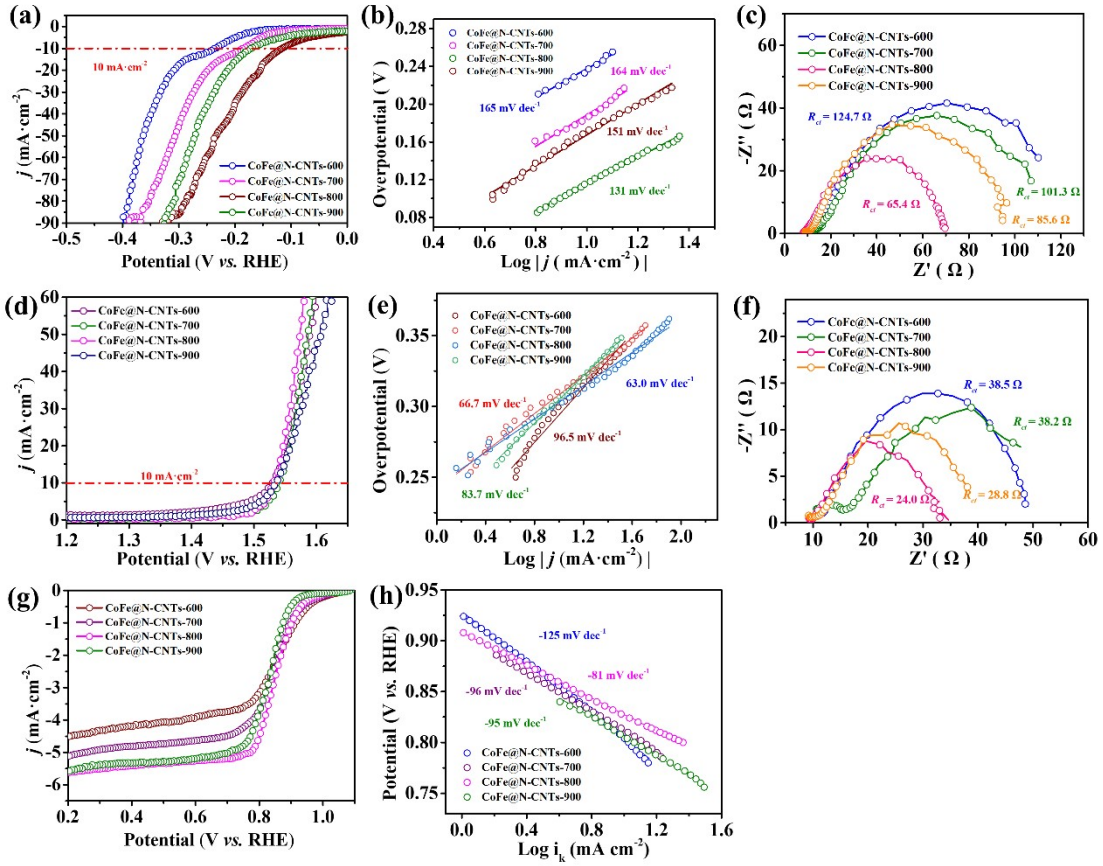

Fig. S6. Comparison of HER electrocatalytic activity of CoFe@N-CNTs-600, CoFe@N-CNTs-700, CoFe@N-CNTs-800, and CoFe@N-CNTs-900: (a) LSV curves, (b) Tafel slopes and (c) EIS spectra for HER; (c) LSV curves, (d) Tafel slopes and (e) EIS spectra for OER; (g) LSV curves and (h) Tafel slopes for ORR.

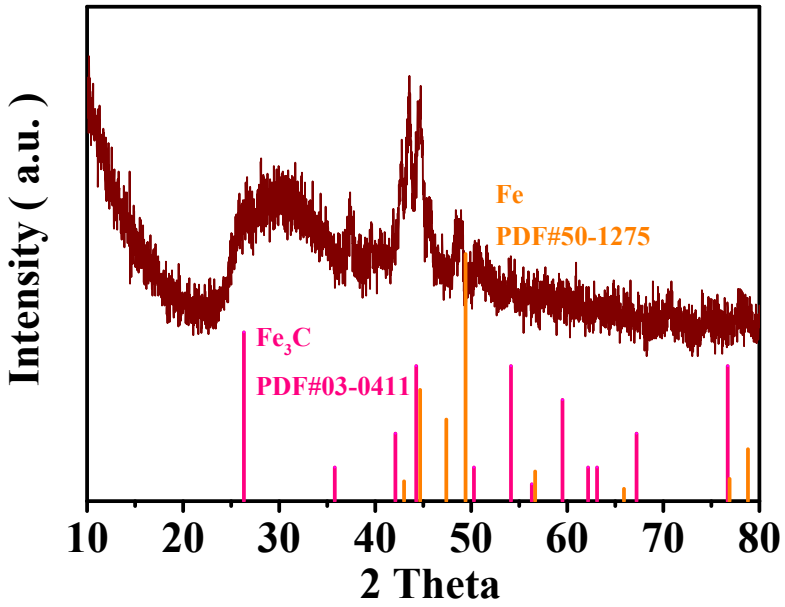

Fig. S7. XRD patterns of A-Fe-PB-800 sample.

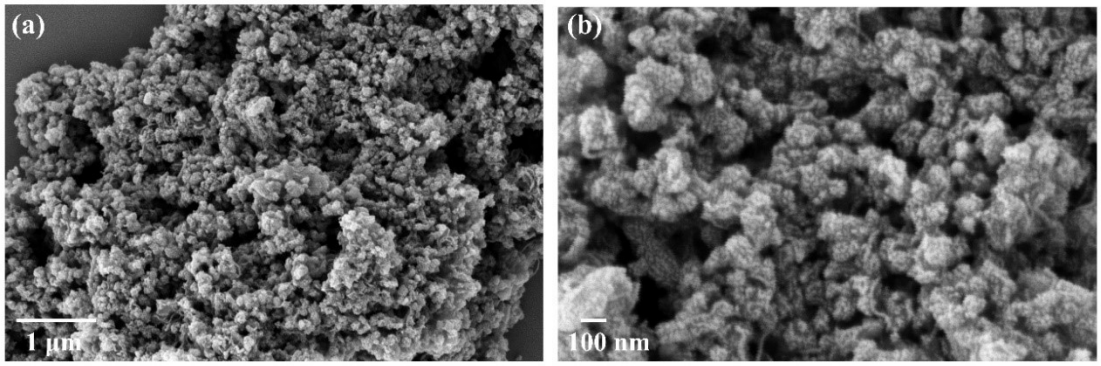

Fig. S8. FESEM images of the as-prepared A-Fe-PB-800 sample.

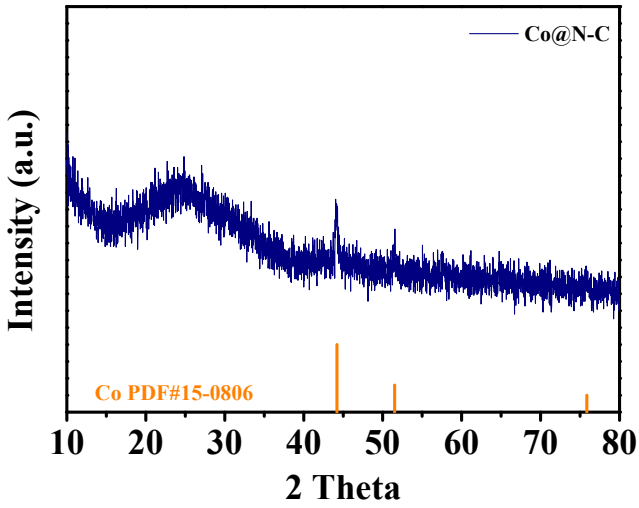

Fig. S9. XRD pattern of A-Co-ZIF-800 sample.

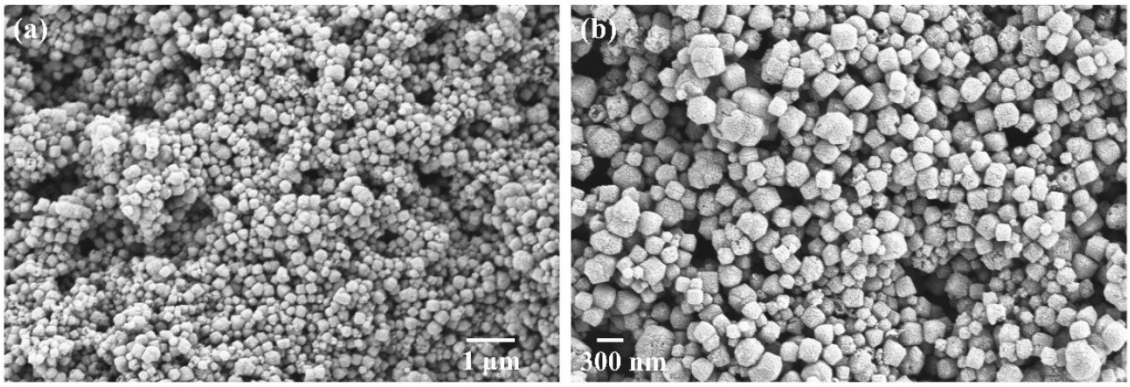

Fig. S10. FESEM images of the as-prepared A-Co-ZIF-800 sample.

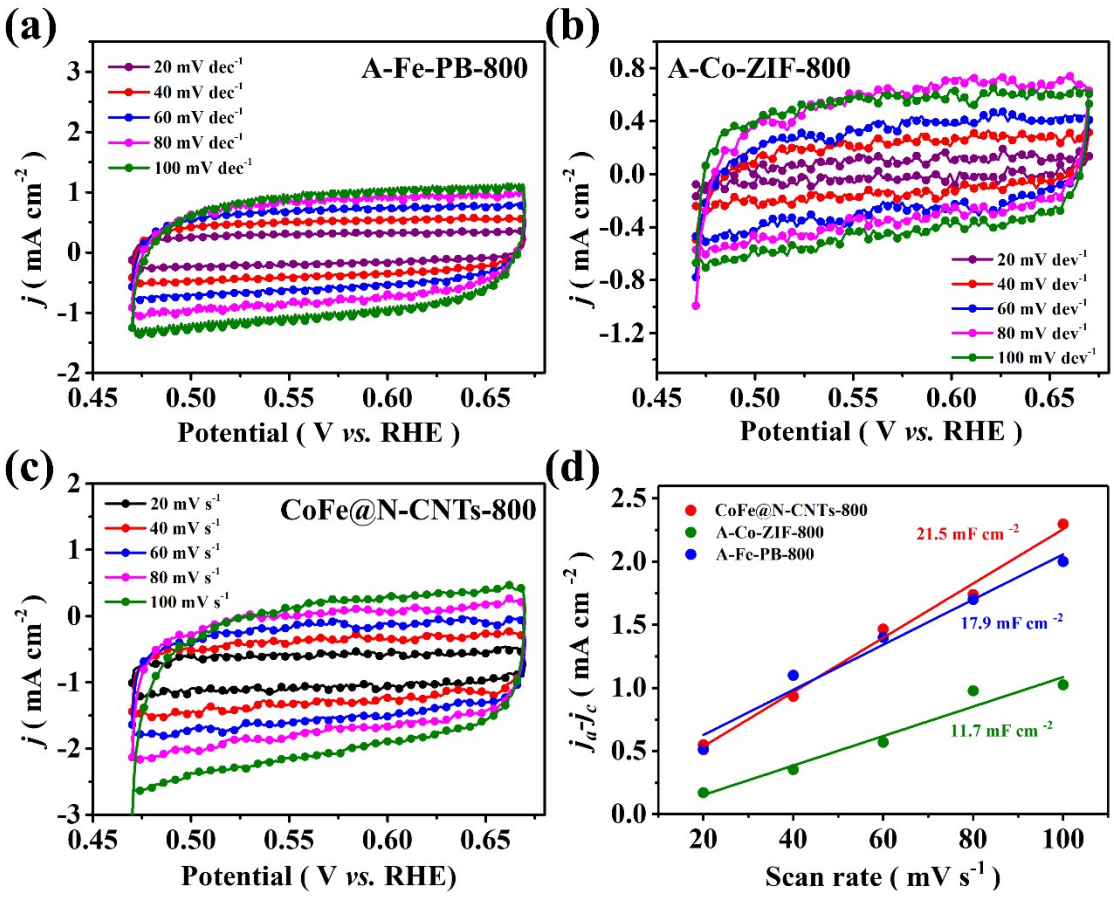

Fig. S11. CV curves for HER within a non-faradaic reaction region of 0.47 ~ 0.67 V *vs.* RHE at different scan rates: (a) A-Fe-PB-800, (b) A-Co-ZIF-800, (c) CoFe@N-CNTs-800, and (d) the corresponding C_{dl}.

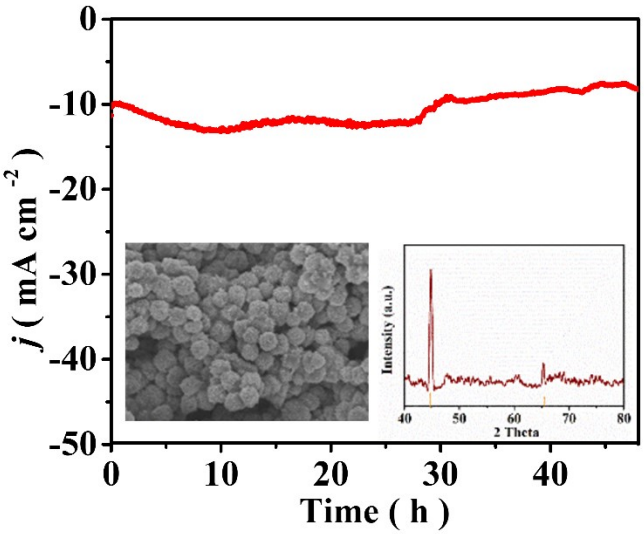

Fig. S12. Electrocatalytic stability tests of CoFe@N-CNTs-800 catalyst: i-t curves for HER (inset: typical FESEM image and XRD pattern of catalyst after 48-hour of the HER stability test).

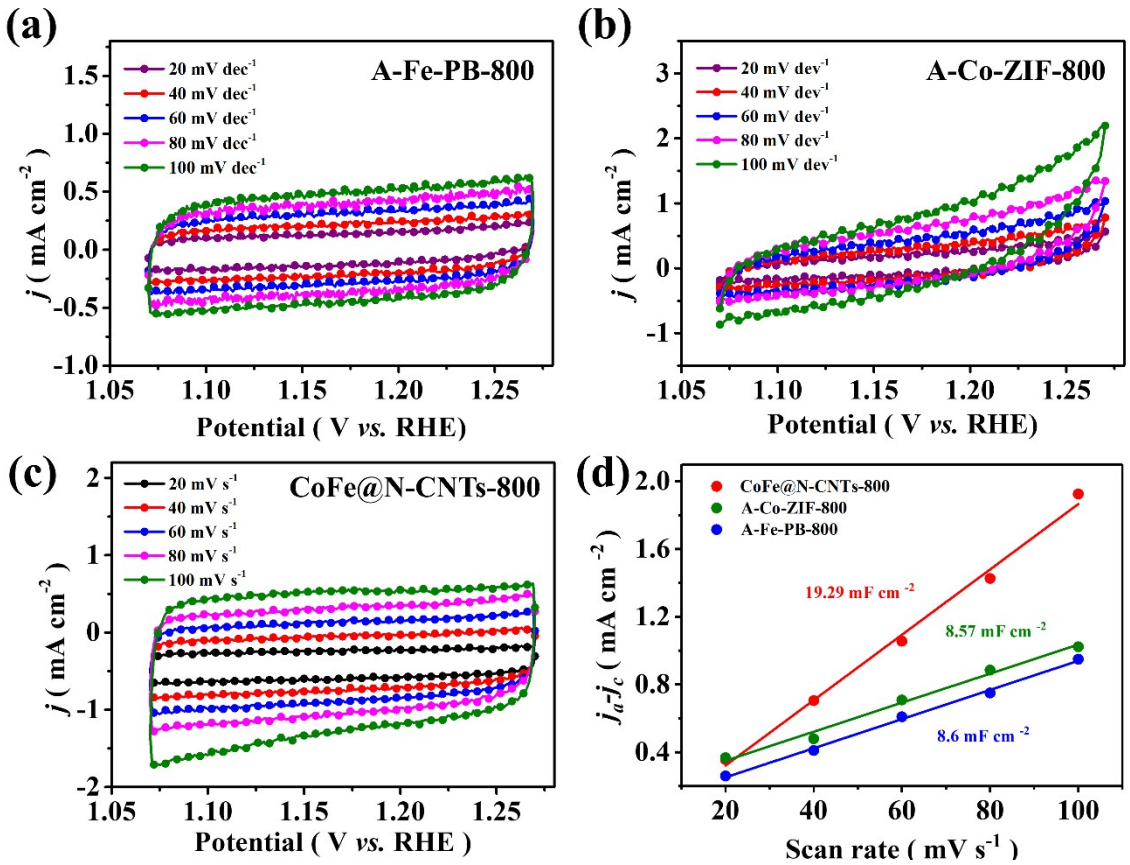

Fig. S13. CV curves for OER within a non-faradaic reaction region of 1.07 ~ 1.27 V *vs.* RHE at different scan rates: (a) A-Fe-PB-800, (b) A-Co-ZIF-800, (c) CoFe@N-CNTs-800, and (d) the corresponding C_{dl}.

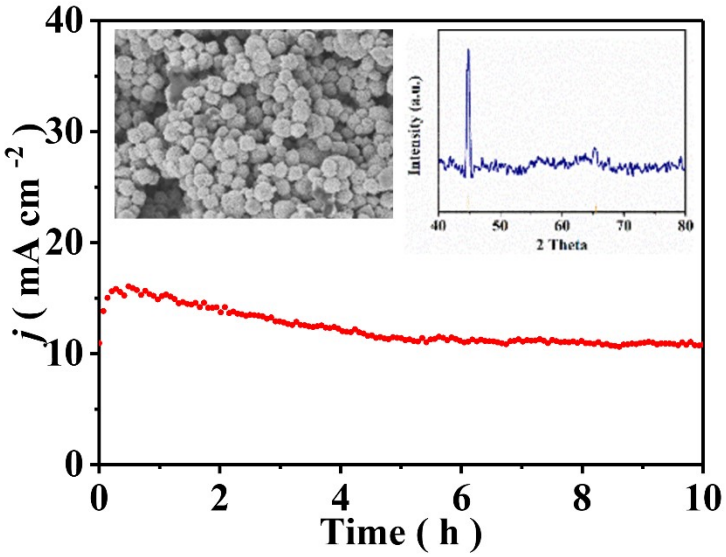

Fig. S14. Electrocatalytic stability test of CoFe@N-CNTs-800 catalyst: i-t curve for OER (inset: typical FESEM image and XRD pattern after 10-hour of the OER stability test).

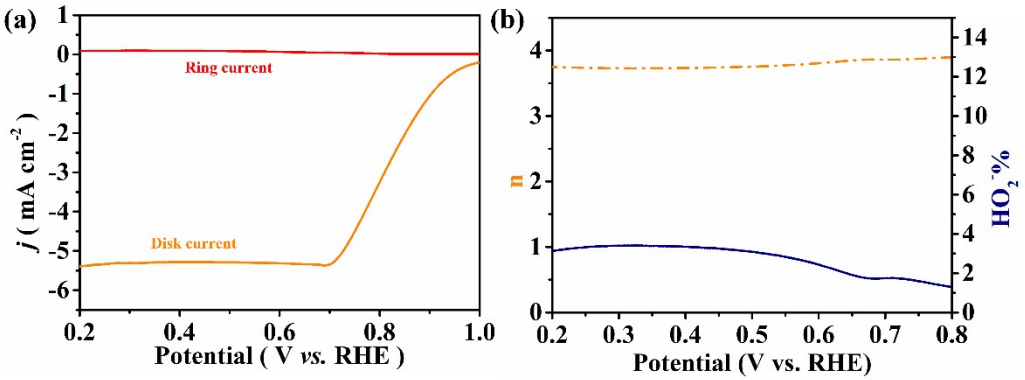

Fig. S15. (a) LSV polarization curves corresponding to the ring current and disk current on CoFe@N-CNTs-800 catalyst. (b) Hydrogen peroxide production rate and electron transfer number curves of CoFe@N-CNTs-800 catalyst.

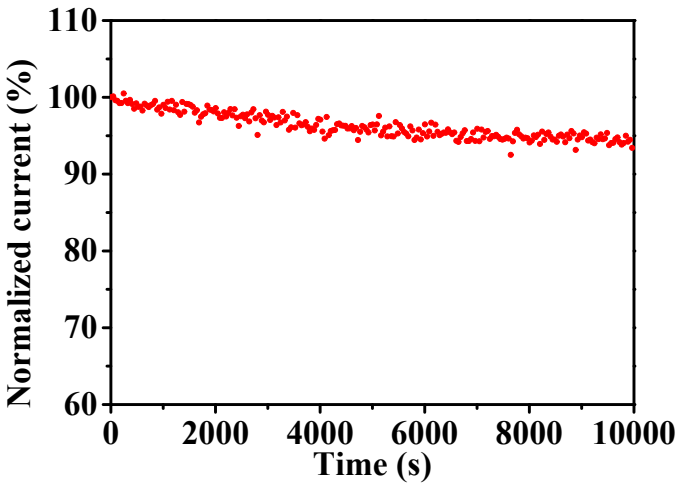

Fig. S16. Electrocatalytic ORR stability test of CoFe@N-CNTs-800 catalyst.

Table S1. Comparison of HER performance of CoFe@N-CNTs-800 electrocatalyst with recently reported bifunctional or trifunctional electrocatalysts.

Catalyst	**Electrolyte**	**(mV)@j ($mA\ cm^{-2}$)**	**Reference**
CoSA+ Co_9S_8@HCNT@GCE SA: single atoms	1 M KOH	250@10	[S1]
Co_9S_8@Co_9S_8@MoS_2-0.5@GCE	1 M KOH	173@10	[S2]
Fe_3C-Co/NC@GCE	1 M KOH	238@10	[S3]
FeCo/Co_2P@NPCF NPCF: N, P- codoped carbon nanofiber	1 M KOH	260@10	[S4]
Co/N-C@GCE	1 M KOH	212@10	[S5]
Co@NCNT@GCE	1 M KOH	244@10	[S6]
Defect Graphene@GCE	1 M KOH	320@10	[S7]
$Fe_{0.5}Co_{0.5}$@NC/NCNS-800@GCE NCNS: N-doped carbon nanosheets	1 M KOH	150@10	[S8]
FeCo-TA@CMS@GCE	1 M KOH	233@10	[S11]
CoFe-N-CNTs-800@GCE	1 M KOH	115@10	This work

Table S2. The corresponding EIS calculation parameters of Fe@N-C, Co@N-C, and CoFe@N-CNTs-800 catalysts for HER.

Sample	**Fe@N-C**		**Co@N-C**		**CoFe@N-CNTs-800**	
Element	**Value**	**Error(%)**	**Value**	**Error(%)**	**Value**	**Error(%)**
Rs (Ω)	8.795	1.241	10.36	1.0894	12.69	2.0308
Rct (Ω)	281.8	3.1356	195.2	3.351	85.6	1.9023
CPE-T (Ω)	0.0011049	3.815	0.0014899	4.1086	0.0014625	4.57
CPE-P (Ω)	0.68809	3.1356	0.7276	1.2766	0.84239	1.4885

Table S3. Comparison of OER performance of CoFe@N-CNTs-800 electrocatalyst with recently reported bifunctional or trifunctional electrocatalysts.

Catalyst	**Electrolye**	**(mV)@j (mA cm^{-2})**	**Reference**
CoSA+Co_9S_8@HCNT@GCE SA: single atom	1M KOH	330@10	[S1]
Co_9S_8@Co_9S_8@MoS_2-0.5@GCE	1 M KOH	340@10	[S2]
Fe_3C-Co/NC@GCE	1 M KOH	340@10	[S3]
FeCo/Co_2P@NPCF NPCF: N, P- codoped carbon nanofiber	0.1 M KOH	330@10	[S4]
Co/N-C@GCE	1 M KOH	400@10	[S5]
Co@NCNT@GCE	1 M KOH	429@10	[S6]
Defect Graphene@GCE	1 M KOH	340@10	[S7]
$Fe_{0.5}Co_{0.5}$@NC/NCNS-800 @GCE NCNS: N-doped carbon nanosheets	1 M KOH	370@10	[S8]
FeCo@MNC@GCE MNC: mesoporous Fe/Co-N-C nanofibers	1 M KOH	240@10	[S9]
FeCo-N-C-700@GCE	1 M KOH	370@10	[S10]
FeCo-TA@CMS	1 M KOH	380@10	[S11]
CoFe-N-CNTs-800@GCE	1 M KOH	306@10	This work

Table S4. The corresponding EIS calculation parameters of Fe@N-C, Co@N-C, and CoFe@N-CNTs-800 catalysts for OER.

Sample	**Fe@N-C**		**Co@N-C**		**CoFe@N-CNTs-800**	
Element	**Value**	**Error(%)**	**Value**	**Error(%)**	**Value**	**Error(%)**
Rs (Ω)	9.904	0.85789	10.72	1.8428	11.57	1.3942
Rct (Ω)	353.9	1.6101	177.2	1.798	28.81	3.0688
CPE-T (Ω)	0.000031869	3.5426	0.00003199	6.9361	0.0018646	8.8185
CPE-P (Ω)	0.83307	1.6101	0.83906	1.0535	0.77294	2.4936

Table S5. Comparison of overall water splitting performance of CoFe@N-CNTs-800 electrocatalyst with recently reported bifunctional or trifunctional electrocatalysts.

Catalyst	**Electrolye**	**$E_{j=10}$**	**Reference**
Co/N-C@GCE	1 M KOH	1.69	[S5]
CoP@FeCoP@GCE	1 M KOH	1.68	[S12]
FeCo/Co_2P@NPCF@GCE	1 M KOH	1.68	[S4]
Fe_3Co_7@PCNSs@GCE (porous carbon nanosheets)	1 M KOH	1.667	[S13]
Al, Fe-codoped CoP@GCE	1 M KOH	1.66	[S14]
FeCoP@NCNFs@GCE (N-doped electrospun carbon nanofibers)	1 M KOH	1.65	[S15]
FeCo-FeCoP@C@NCCs@GCE	1 M KOH	1.64	[S16]
CoFe@N-CNTs-800@GCE	1 M KOH	1.64	This work

Table S6. Comparison of ORR performance of CoFe@N-CNTs-800 electrocatalyst with recently reported bifunctional or trifunctional electrocatalysts in 0.1 M KOH solution.

Catalyst	**E_0 (V) *vs.* RHE**	**$E_{1/2}$ (V) *vs.* RHE**	**n**	**Reference**
CoSA+Co_9S_8@HCNT@GCE SA: single atom	/	0.855	3.98	[S1]
Co_9S_8@Co_9S_8@MoS_2-0.5@GCE	/	0.776	3.5-4	[S2]
Fe_3C-Co/NC@GCE	0.94	0.885	3.9	[S3]
FeCo/Co_2P@NPCF	0.85	0.79	3.85	[S4]
Co/N-C@GCE	0.97	0.88	3.81-3.99	[S5]
Co@NCNT@GCE	1.03	0.828	3.9	[S6]
Defect Graphene@GCE	0.91	0.76	3.9	[S7]
FeCo@MNC@GCE	/	0.88	3.87	[S9]
FeCo-N-C-700@GCE	1.013	0.896	3.96-3.99	[S10]
FeCo-TA@CMS	0.95	0.83	3.8	[S11]
CoFe-N-CNTs-800@GCE	0.931	0.847	3.7-3.9	This work

Reference

[S1] Y. Z. Li, R. Cao, L. B. Li, X. N. Tang, T. L. Chu, B. Y. Huang, K. Yuan, and Y. W. Chen, *Small*, 2020, **16**, 1906735.

[S2] J. Li, G. S. Li, J. H. Wang, C. L. Xue, X. S. Li, S. Wang, B. Q. Han, M. Yang, and L. P. Li, *Inorg. Chem. Front.*, 2020, **7**, 191.

[S3] C. C. Yang, S. F. Zai, Y. T. Zhou, L. Du, and Q. Jiang, *Adv. Funct. Mater.*, 2019, **29**, 1901949.

[S4] Q. Shi, Q. Liu, Y. Ma, Z. Fang, Z. Liang, G. Shao, B. Tang, W. Y. Yang, L. Qin, and X. S. Fang, *Adv. Energy Mater.*, 2020, **10**, 1903854.

[S5] Z. Pei, Z. Tang, Z. Liu, Y. Huang, Y. Wang, H. Li, Q. Xue, M. Zhu, D. Tang, and C. Zhi, *J. Mater. Chem. A*, 2018, **6**, 489.

[S6] E. Zhang, Y. Xie, S. Ci, J. Jia, P. Cai, L. Yi, and Z. Wen, *J. Mater. Chem. A,* 2016, **4**, 17288.

[S7] Y. Jia, L. Zhang, A. Du, G. Gao, J. Chen, X. Yan, C. L. Brown, and X. Yao, *Adv. Mater.*, 2016, **28**, 9532.

[S8] M. Li, T. T. Liu, X. J. Bo, M. Zhou, and L. P. Guo, *J. Mater. Chem. A*, 2017, **5**, 5413.

[S9] L. Cong, M. C. Li, and R. L. Wu, *Appl. Catal. B: Environ.*, **2019**, 244, 150.

[S10] X. D. Duan, S. S. Ren, N. Pan, M. D. Zhang, and H. G. Zheng, *J. Mater. Chem. A*, 2020), **8**, 9355.

[S11] H. Liu, D. H. Yang, X. Y. Wang, J. W. Zhang, and B. H. Han, *J. Colloid Interface Sci.*, 2021, **581**, 362.

[S12] J.H. Shi, F. Qiu, W. B. Yuan, M. M. Guo, and H. L. Zhan, *Chem. Eng. J.*, 2021, **403**, 126312.

[S13] T. T. Liu, M. Li, X. J. Bo, and M. Zhou, *J. Colloid Interface Sci.*, 2019, **537**,

280.

[S14] S. F. Zai, Y. T. Zhou, C. C. Yang, and Q. Jiang, *Chem. Eng. J.*, 2021, **421**, 127856.

[S15] B. Wei, G. C. Xu, J. C. Hei, L. Zhang, and T. T. Huang, *Int. J. Hydrog. Energy*, 2021, **46**, 2225.

[S16] Y. Z. Li, S. W. Li, Hu J, Y. Y. Zhang, Y. C. Du, X. J. Han, X. Liu, and P. Xu, *J. Energy Chem.*, 2021, **53**, 1.